Automatic Detection and Characterization of Closely-Spaced Objects

Brandoch Calef
The Boeing Company, Kihei, HI
Shadi Naderi
Directed Energy Directorate, Air Force Research Laboratory,
Air Force Maui Optical and Supercomputing (AMOS) Site, Kihei, HI

ABSTRACT

We present a system developed at AMOS to perform automated closely-spaced object (CSO) detection and characterization. The approach is based on speckle interferometry, a mature technique whereby high-spatial frequency information is recovered from a sequence of short-exposure images. To characterize its performance, we present observations of hundreds of binary stars drawn from the Washington Double Star catalog and TESS exoplanet candidate systems using imaging sensors on the AMOS 1.6 and 3.6 meter telescopes. These demonstrate its ability to detect companions at angular separations approaching the diffraction limit, equivalent to a projected separation on the order of 5 meters at GEO range. Finally, we present observations of cooperative satellites performing proximity operations.

1. INTRODUCTION

A basic aspect of space domain awareness is the ability to detect and characterize objects in proximity to satellites of interest. In the context of GEO satellites being monitored by ground-based optical telescopes, this "closely-spaced object" (CSO) problem is made challenging by the faintness of the objects and limits on angular resolution imposed by atmospheric blurring and the diffraction limit of the optical system. This paper describes CSO experiments performed at AMOS based on the use of speckle interferometry, which is a class of techniques that allow the recovery of high-spatial frequency information from a sequence of short-exposure images. Speckle interferometry does not require adaptive optics (AO), so it remains useful in situations where there is not enough light for passive AO and it is impractical to operate a laser guidestar.

2. APPROACH

We begin by briefly reviewing the basic concepts of speckle interferometry. Consider an object scene (i.e. a spatial distribution of light in the target plane) $o(x)$ observed through the atmosphere, which causes approximately spatially-invariant blurring with some point-spread function (PSF) $h(x)$. Naturally, the atmospheric PSF changes as a function of time. Assume that any changes in the object are much slower than the characteristic time of the atmosphere. The instantaneous intensity at the focal plane of the optical system is then the convolution $d(x) = (o * h)(x)$. Integrating over time yields a long-exposure image $\langle d \rangle = (o * \langle h \rangle)(x)$. In large-aperture telescopes, the spatial frequency content of $\langle h \rangle$ is limited by atmospheric turbulence rather than the diffraction limit. However, in the early days of speckle interferometry, Labeyrie [1] observed that a power spectrum estimate formed from short exposures *does* preserve information out to the diffraction limit. Writing $O(u)$, $H(u)$, and $D(u)$ as the Fourier transforms of $o(x)$, $h(x)$, and $d(x)$, respectively, the measured quantity is

$$\langle |D(u)|^2 \rangle = |O(u)|^2 \langle |H(u)|^2 \rangle, \tag{1}$$

from which it is evidently possible to recover $|O|$ if the speckle transfer function (STF) $\langle |H|^2 \rangle$ is known. The STF can be obtained by observing a point source (such as a star), where $|O| = 1$.

Once the modulus of the O is known, it only remains to recover its phase, e.g. from the cross spectrum [2] or bispectrum [3]. The bispectrum of an image $d(x)$ with Fourier transform $D(u)$ is a function of two spatial frequency variables u, v defined by

$$B_D(u,v) = D(u)\, D(v)\, D^*(u+v). \tag{2}$$

Approved for public release; distribution unlimited. Public affairs approval AFRL-2022-4122.

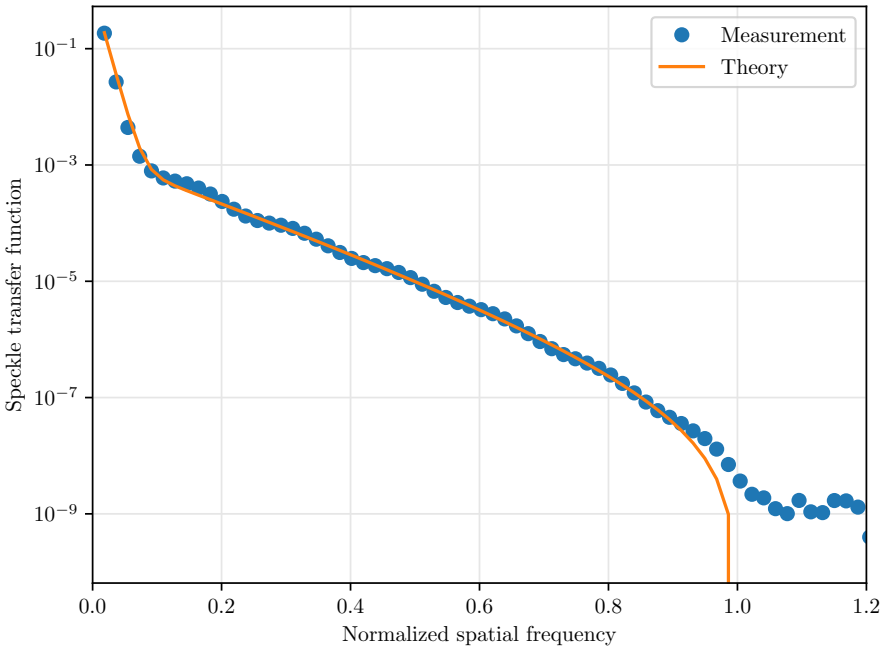

Fig. 1: STF estimate formed during observation of WDS 00352-0336.

The expected bispectrum of the measured data is therefore

$$\langle B_D(u,v)\rangle = B_O(u,v)\,\langle B_H(u,v)\rangle, \tag{3}$$

where O is the Fourier transform of the object o and H is the Fourier transform of the PSF h. It can be shown that second term on the right-hand side (the expected bispectrum of the atmospheric PSF) has zero phase but nonzero modulus, provided u, v, and $u+v$ are within the diffraction limit. Therefore, the phase of the expected bispectrum of the measured data is exactly the phase of the bispectrum of the target:

$$\arg\langle B_D(u,v)\rangle = \arg B_O(u,v). \tag{4}$$

There are various ways of recovering the Fourier phase of the image from the bispectrum phase, for example using the recursion

$$\arg O(0) = 0 \tag{5}$$
$$\arg O(\pm 1,0) = 0 \tag{6}$$
$$\arg O(0,\pm 1) = 0 \tag{7}$$
$$\arg O(u+v) = \arg O(u) + \arg O(v) - \arg\langle B_D(u,v)\rangle \tag{8}$$

suggested by Eqn. 2.

The CSO problem may be formulated as a special case where the object is a sum of a finite number of point sources (usually two). In this case, the power spectrum of the object is a sinusoid whose frequency is inversely proportional to the separation between the sources. Our approach to this problem is inspired by the work of astronomers studying binary stars, especially Tokovinin (e.g. [4]) and Horch and collaborators (e.g. [5]).

First, the STF $\langle |H|^2\rangle$ is estimated by fitting the theoretical response to the azimuthally averaged measured spectrum, as illustrated in Fig. 1. Next, the power spectrum $|O|^2$ is estimated and Fourier transformed to yield the autocorrelation of the object. Local peaks in the autocorrelation are detected by looking for 5σ outliers as a function of distance in

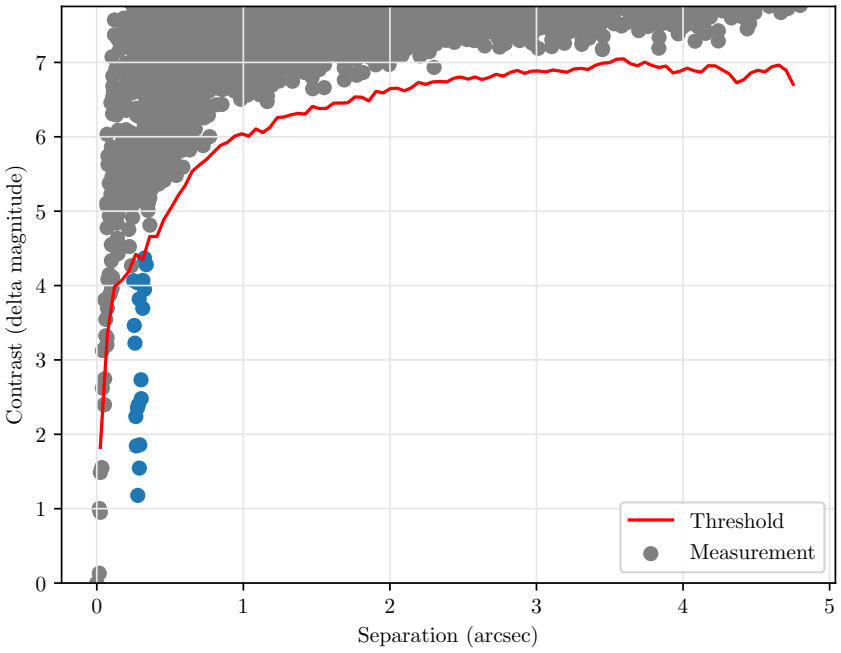

Fig. 2: Detection limit as function of separation. The blue dots are outliers corresponding to the companion star in WDS 00352-0336.

the autocorrelation. This also yields a detection threshold as a function of separation, as illustrated in Fig. 2. These local peaks are then used to seed a maximum likelihood fit of the sinusoidal fringe pattern to the power spectrum (see Fig. 3). This yields an estimate of the contrast (delta-magnitude) between the objects and their separation, although from the power spectrum alone it is impossible to determine the sign of the separation (i.e. which object is which). To resolve this ambiguity, the Fourier phase is recovered from the bispectrum and a reconstructed image is formed (Fig. 4). Since the bispectrum has lower SNR than the power spectrum, there are marginal cases in which this last step is impossible, and it is only possible to recover the position angle modulo 180°.

3. OBSERVATIONS

Using AMOS telescopes, we have observed many binary and multiple star systems as well as a handful of nights of cooperative satellites conducting proximity operations. Most of the observations reported here were carried out on the ARDI sensor on the AEOS 3.6 meter telescope. The plate scale was measured each night using calibration binaries and found to be consistently about 82.7 nrad/pixel. The majority of the ARDI observations were made in an 850 nm shortpass filter, which is very broad compared to most published work on binary stars, but in practice delivered better results than the other filters we tried. The integration time was typically 100 msec, going to shorter exposures when the signal threatened to saturate the camera. Every dataset consists of 50 seconds worth of short-exposure frames. The data were collected and processed by a fully automated system.

3.1 ORB6 Catalog Stars

To evaluate the performance of the approach, we used the Sixth Catalog of Orbits of Visual Binary Stars (ORB6) [6] as a source of test targets. As illustrated in Fig. 5, we obtained excellent agreement with the catalog separations, with RMS error of about 3 milliarcseconds in separation for grade 1 and 2 orbits at separations greater than $2\lambda/D$.

Since the object is parameterized as a sum of two point sources rather than a general extended source, it is possible to detect companions at separations less than λ/D, but we find that there is a positive bias in the separation estimate in

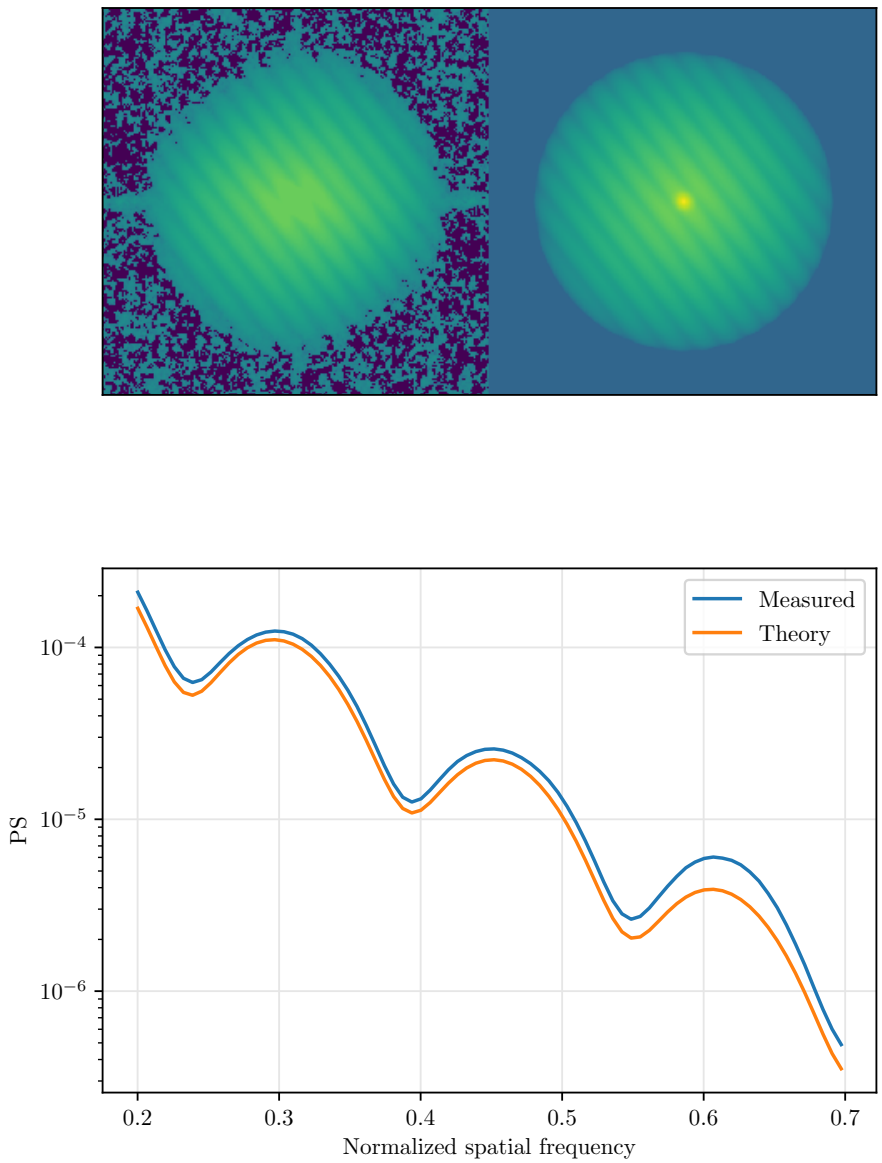

Fig. 3: Power spectrum measured vs. modeled.

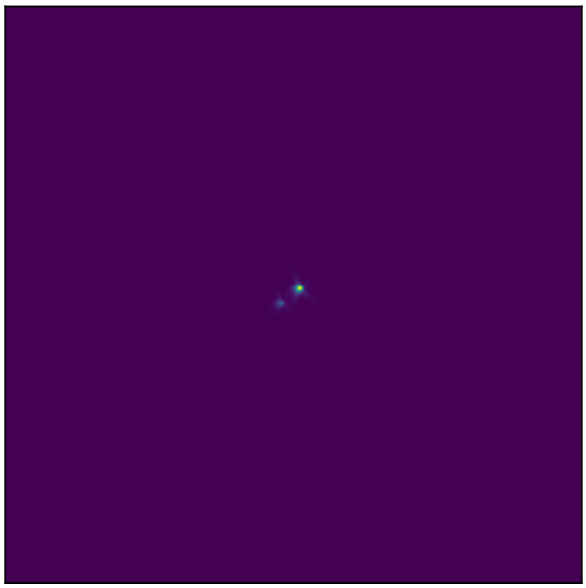

Fig. 4: Reconstructed image of WDS 00352-0336.

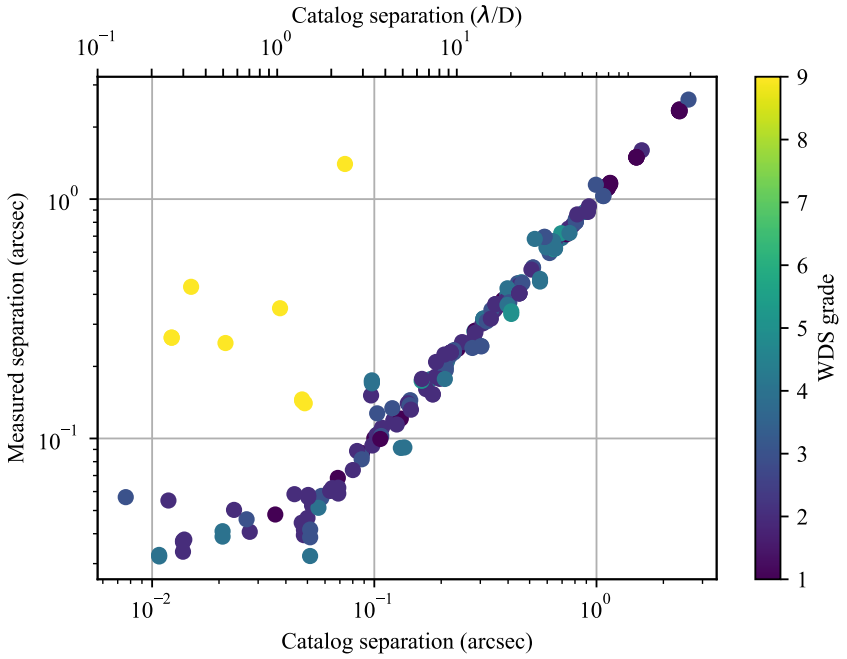

Fig. 5: ORB6 separation bias. Note the positive bias for cases separated by less than λ/D. Also note the large error for ORB6 grade 9 systems, suggesting error in the catalog.

Table 1: TOI observations. Systems marked with † have questionable parity (θ could be off by 180°). Systems marked with * are reported here for the first time.

TOI	mag(TESS)	Date	ρ (arcsec)	θ (deg)	Δmag
1142	8.64	2022.3179*	0.994	171.25	2.61
1152	8.03	2022.3288	1.566	166.52	0.44
1351	10.33	2022.3180*	0.922	225.35	0.87
1697	11.17	2022.3181	1.885	139.02	3.04
2138	12.55	2022.3179*	0.199	215.02†	1.65
2256	10.45	2022.3179	0.281	299.81†	1.58
			0.375	301.21†	1.29
3569	11.02	2022.3182	0.254	236.45	0.46
3921	12.56	2022.3179*	2.936	47.26	2.22
			5.185	24.56	3.81
4045	13.22	2022.3181*	0.323	45.08	0.67
4089	11.64	2022.3289	1.133	59.63	1.97
4389	9.50	2022.3179	0.150	63.03	0.51

these cases. This may be due to the extreme sensitivity of the estimate to inconsistency in the STF approximation at the highest spatial frequencies.

3.2 TESS Exoplanet Candidate Systems

As a further source of interesting targets, we observed a random selection of the TESS Object of Interest (TOI) [7] list of exoplanet candidates. Of the roughly 150 collections, nine were binary systems and two were ternary (see Table 1). Of these, five (indicated with an asterisk in the table) had no previous reported observations on the ExoFOP web site.

3.3 Satellites

We observed satellites in near-GEO conducting proximity operations. For these collections, the 3.6 meter telescope was unavailable, so we instead used the FLASH sensor on the 1.6 meter telescope. The observing procedure was essentially the same as for the star collections. The encounter is summarized in Figs. 6 and 7. Figure 6 shows separation and relative brightness as a function of time. Around 1200 seconds, the companion object became much fainter and was not detected for about 300 seconds. Near closest approach, the companion was lost again for another 300 seconds. The closest detection was at 0.15 arcsec (about $1.5\lambda/D$). Figure 7 shows a handful of images of the two satellites during the RPO. Interpolating the measured separations suggests that the closest projected separation between the two satellites was about 0.026 arcsec.

4. CONCLUSIONS

We have implemented a system to detect closely spaced objects using speckle imaging sensors on the AMOS telescopes. Testing on hundreds of catalog binary stars shows that the system is robust and accurate to about $2\lambda/D$, and at closer separations it continues to detect companions but reports the separation estimates are less reliable. Finally, we have exercised the system during observations of satellites conducting proximity operations.

5. ACKNOWLEDGEMENTS

This research has made use of the Exoplanet Follow-up Observation Program website, which is operated by the California Institute of Technology, under contract with the National Aeronautics and Space Administration under the Exoplanet Exploration Program.

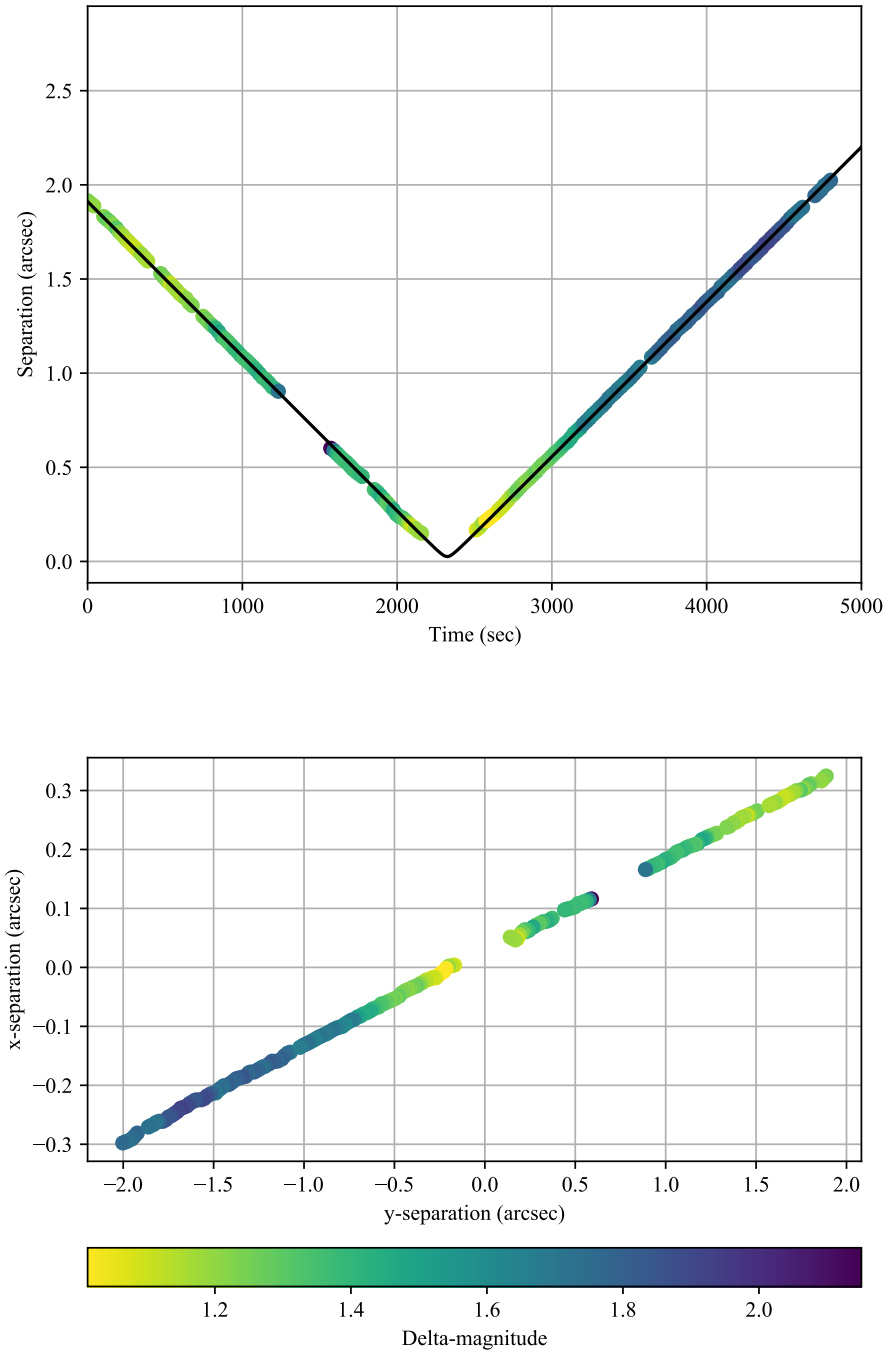

Fig. 6: Separation (top) and relative position (bottom) of satellites conducting proximity operations.

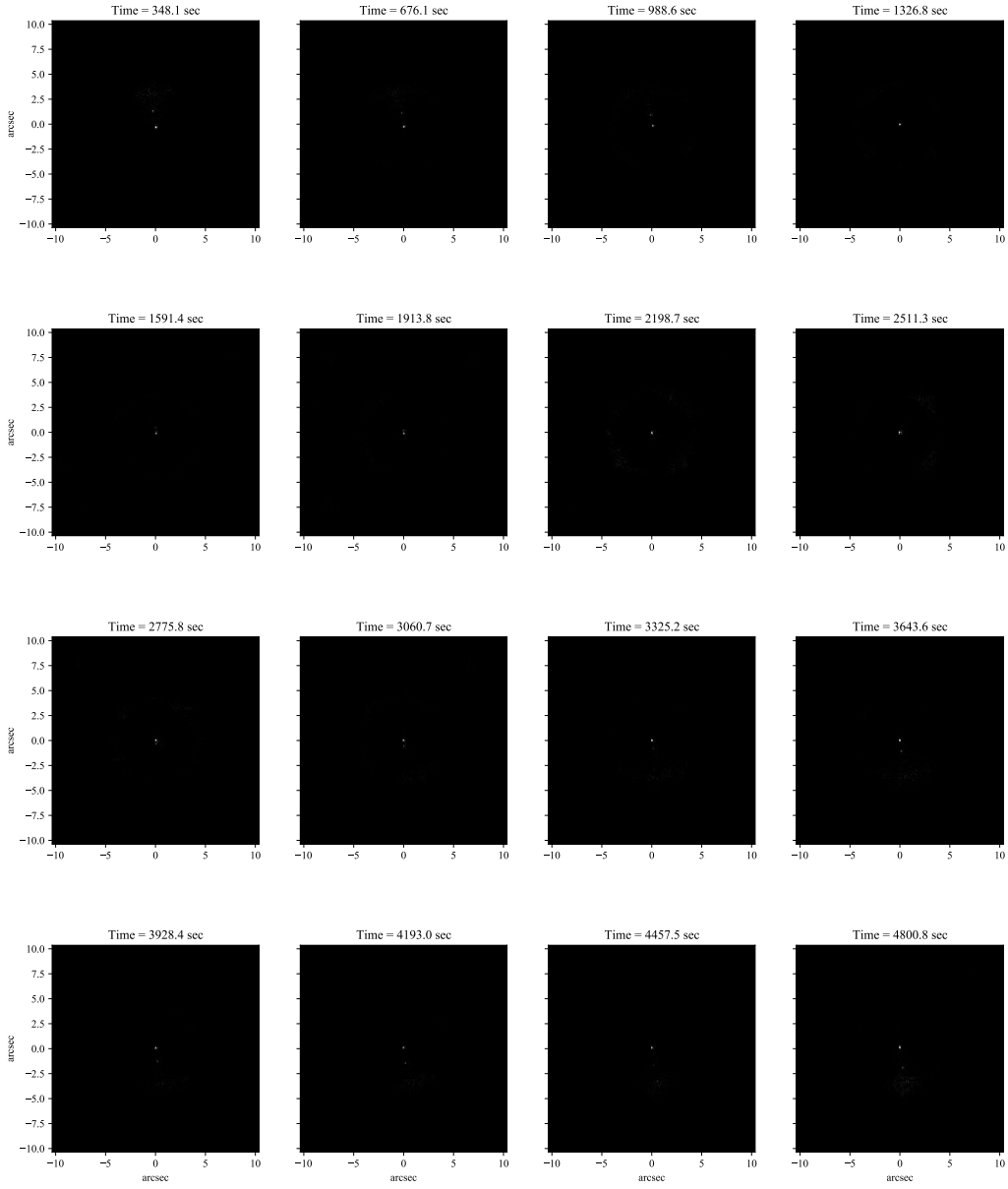

Fig. 7: Reconstructed images of satellites during RPO.

REFERENCES

[1] Antoine Labeyrie. Attainment of diffraction limited resolution in large telescopes by Fourier analysing speckle patterns in star images. *Astronomy and Astrophysics*, 6:85, 1970.

[2] Keith T. Knox and Brian J. Thompson. Recovery of images from atmospherically degraded short-exposure photographs. *The Astrophysical Journal*, 193:L45–L48, 1974.

[3] Adolf W. Lohmann, Gerd Weigelt, and Bernhard Wirnitzer. Speckle masking in astronomy: triple correlation theory and applications. *Applied Optics*, 22(24):4028–4037, 1983.

[4] Andrei Tokovinin. Ten years of speckle interferometry at SOAR. *Publications of the Astronomical Society of the Pacific*, 130(985):035002, 2018.

[5] Elliott P. Horch, Gerard T. van Belle, James W. Davidson Jr, Lindsay A. Ciastko, Mark E. Everett, and Karen S. Bjorkman. Observations of binary stars with the differential speckle survey instrument. VI. Measures during 2014 at the Discovery Channel Telescope. *The Astronomical Journal*, 150(5):151, 2015.

[6] Rachel A. Matson, Stephen J. Williams, William I. Hartkopf, and Brian D. Mason. Sixth catalog of orbits of visual binary stars. `http://www.astro.gsu.edu/wds/orb6.html`, 2022.

[7] ExoFOP. Exoplanet follow-up observing program - TESS. `https://exofop.ipac.caltech.edu/tess/`.